Atomistic Mechanism of Friction-Force Independence on the Normal Load and Other Friction Laws for Dynamic Structural Superlubricity

Nikolay V. Brilliantov,[1,2] Alexey A. Tsukanov,[3] Artem K. Grebenko,[4] Albert G. Nasibulin,[1,5] and Igor A. Ostanin[6]
[1]*Skolkovo Institute of Science and Technology, 121205 Moscow, Russia*
[2]*Department of Mathematics, University of Leicester, Leicester LE1 7RH, United Kingdom*
[3]*Research and Development Center, TerraVox Global, Paphos, Cyprus*
[4]*Centre for Advanced 2D Materials, National University of Singapore, Singapore*
[5]*Kemerovo State University, Krasnaya 6, 650000, Kemerovo, Russia*
[6]*Faculty of Engineering Technology, University of Twente, 7500 AE Enschede, The Netherlands*

(Received 8 February 2023; revised 7 July 2023; accepted 14 November 2023; published 26 December 2023)

We explore dynamic structural superlubricity for the case of a relatively large contact area, where the friction force is proportional to the area (exceeding $\sim$100 nm^2) experimentally, numerically, and theoretically. We use a setup composed of two molecular smooth incommensurate surfaces: graphene-covered tip and substrate. The experiments and molecular dynamic simulations demonstrate independence of the friction force on the normal load for a wide range of normal loads and relative surface velocities. We propose an atomistic mechanism for this phenomenon, associated with synchronic out-of-plane surface fluctuations of thermal origin, and confirm it by numerical experiments. Based on this mechanism, we develop a theory for this type of superlubricity and show that friction force increases linearly with increasing temperature and relative velocity for velocities larger than a threshold velocity. The molecular dynamic results are in a fair agreement with predictions of the theory.

DOI: 10.1103/PhysRevLett.131.266201

Introduction.—Understanding physical nature of friction at different scales, including nanoscales, and ability to control it, is of immense fundamental and practical importance [1,2]. Indeed, nearly a quarter of irreversible energy losses of today's world industry is attributed to friction [3,4]. Therefore superlubricity—the ultralow friction due to mutual cancellations of tangential forces for incommensurate surfaces [5,6]—seems to be very promising for future technical applications. It was first predicted theoretically [7,8] and then confirmed experimentally, e.g., [9–14], and numerically, e.g., [14–16].

Superlubricity has been reported for many nanoscale and microscale systems, ranging from junctions of multilayer graphene flakes and graphite surface, graphene, or graphitic junctions to graphene or graphite-boron nitride heterojunctions [9–16]. There exists, however, a number of effects that restrict superlubricity. Among these are incomplete cancellation of tangential forces due to incomplete unit cells of the arising moiré pattern at the rim area of the layer (finite size effects), as well as incomplete cancellation within complete unit cells [17–19], atomic scale defects [20], and motion of domain walls in superstructures with large commensurate domains [21]. These effects may give rise to static and dynamic friction. Moreover, superlubricity may be destroyed [15] by spontaneous variation of surface orientation, resulting in a commensurate state [22] owing to load-induced commensuration [15,23] or other similar effects, e.g., [24].

Most of the above restrictions may be, in principle, surmounted by improving technology, e.g., by diminishing atomic scale defects, decreasing role of the rim area, or increasing the contact size, as demonstrated in Ref. [19]. Still there exists a restriction for dynamic superlubricity, which remains even for an ideal case of complete incommensurability and negligible role of finite-size effects. It stems from unavoidable corrugation of the contacting surfaces due to out-of-plane thermal fluctuations of the surfaces. The importance of such surface deformation for friction has been demonstrated in [25] for a coarse-grained model of atomic graphene film sandwiched between two metal surfaces.

Here, we address the dynamic friction in structurally superlubric systems for contacting incommensurate surfaces due to corrugation of the surfaces by out-of-plane thermal fluctuations. We consider the case of relatively large incommensurate contacts when friction due to rim effects, restricting superlubricity, is small as compared to friction due to out-of-plane fluctuations. This corresponds to the "solitonlike, smooth sliding" regime, according to

classification of Ref. [19]. Hence, it differs from the most of the studies of dynamic superlubricity, mainly focused on "coherent stick-slip" or "collective stick-slip" regimes [19], which refer to relatively small contacts. Physically, the addressed mechanism is similar to the one proposed for commensurate molecularly smooth surfaces of two concentric carbon nanotubes performing relative telescopic motion [26,27].

We investigate such systems experimentally, and by large-scale molecular dynamic (MD) simulations. Unlike previous studies, we mimic the experimental setup using the atomistic (and not coarse-grained) model, along with the most realistic, recent interatomic potentials. Also, we develop a theory of such kind of dynamic superlubricity. In contrast to the previous theories, which assume the friction mechanisms associated with Prandtl-Tomlinson model with thermal activation, e.g., [5,22,28–30] or Frenkel-Kontorova-Tomlinson model, e.g., [8,31], we propose the mechanism of synchronic out-of-plane fluctuations (see below) and confirm it numerically. Based on this mechanism we explain (i) the observed independence of the friction force on the normal load and other friction laws, such as (ii) the increase of the friction force with temperature and relative velocity of contacting surfaces (linear above some velocity threshold), and (iii) a linear proportionality of the force with the true contact area. Although friction independence on the normal load has been reported [13,14,32] (for somewhat smaller range of parameters), as well as proportionality of the friction force to the contact area [14] and its increase with temperature [16], the respective theoretical description of all these laws, as a consequence of a specific mechanism, has not been given.

Experimental results.—We performed experiments by means of lateral force microscopy—the regime of the atomic force microscopy (AFM) designed to explore frictional phenomena at the nanoscale. This method has been successfully utilized before, including the case of graphene over graphene friction studies that support our findings [32–34]. The measurements were performed in N_2 atmosphere with the content of O_2 and H_2O less than 1 ppm. A typical custom multilayer (Si-Ta-Cu/Si-Pd) probe with graphene on the top is shown in Fig. 1(a). For technical details regarding the fabrication and measurements, see Supplemental Material (SM) [35]. In short, we utilized a metallic substrate covered, with a chemical vapor deposition [47] grown, monolayer graphene and silicon probe covered by metal and graphene synthesized via the same chemical vapor deposition technique; we estimate the contact area to be about 10^2–10^3 nm^2 (see SM).

The experimental results presented in Figs. 1(b)–(d), demonstrate very low friction corresponding to structural superlubricity of incommensurate contact. They clearly indicate that, within the accuracy of our measurements, the lateral friction force F_f does not depend on the normal force, F_N, up to several μN, until the graphene coverage of

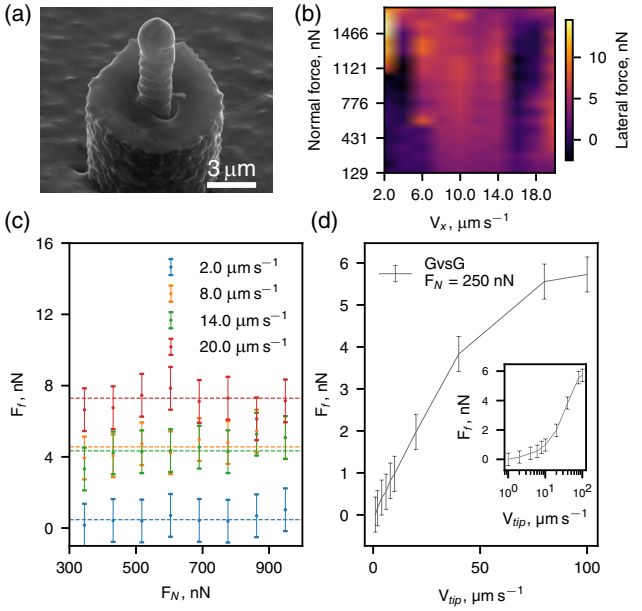

FIG. 1. Friction experiments by means of AFM. (a) SEM image of the AFM probe covered with copper-graphene composite. (b) Lateral force map illustrating its dependence on the normal force (F_N) and tip's velocity (V_{tip}). (c) Friction force, F_f, versus normal load, F_N, for different tip velocities. (d) The dependence of the friction force on the tip's velocity; the inset shows $F_f(V_{tip})$ with logarithmic velocity scale.

the tip remains stable (see also the discussion in SM). The friction force increases with the velocity of the tip, up to $V_{tip} \sim 100$ μm s^{-1}, much faster than logarithmically but somewhat slower than linearly; see Fig. 1(d). Note that the velocities in Ref. [14], where the logarithmic dependence of F_f on V_{tip} was observed, were 2 orders of magnitude smaller. From our results we conjecture that the static friction is vanishingly small.

MD simulations.—We performed numerical experiments for the model depicted in Fig. 2(a), which mimics the above experimental setup, up to the presence of N_2 atmosphere (we assume that its impact is negligible). Its bottom part is a planar graphene nanosheet adhered on the surface (111) of Cu (copper) substrate. The upper part, which models the tip, is a spherical fragment of copper of the initial radius of 300 A°; it is coated by a circular piece of graphene with the radius of about 100 A°. We use incommensurate orientation of the two surfaces; the contact area always exceeded 90 nm^2 (see SM). We varied the normal load F_N by 3 orders of magnitude, from 0.008 to 7.654 nN. The tip was pulled with a constant lateral velocity $V_x = V$, varying from 0.1 to 5 A°/ps. This range of sliding velocities has been chosen to guarantee the acceptable simulation accuracy. Smaller velocities yielded too noisy data for the friction force, while the thermostating lost stability for larger velocities. The MD simulations have been performed for three different temperatures: $T = 320$, 470, and 670 K.

The interactions for graphene were modeled with the use of both the second-generation reactive empirical bond order potential [48] for intralayer C-C interaction, as well as the (refined) Kolmogorov-Crespi potential [49,50] for interlayer C-C interactions between two different layers. For copper we used the embedded atom method [51,52], with the potential developed in [53]. For C-Cu interaction the Abell-Tersoff potential, derived for graphene on Cu substrate, has been employed [54]. The horizontal dimensions of the computational cell were 229.88×193.90 A° (in x and y axis), and about 85 A° in height (z axis). The periodic boundary conditions have been applied along x and y axis. The total number of atoms was 261 064. The bottom half of the substrate and upper half of the tip were coupled to thermostats with temperature T; this yields constant T and unperturbed thermal fluctuations at the surface (see SM). The friction force was computed as a time-averaged x component of the total force acting on the upper part of the system. We have checked that the graphene layers were firmly attached to the according substrates, and formed together a joint solid body. For more computational detail, see SM.

The simulation results are presented in Figs. 2(b)–(e). As it may be seen from the figures, the MD results confirm the experimental observation of practical independence of frictional force on the normal load. Note that the "true" atomic contact area, S, remains almost constant for the studied range of loads, slightly increasing for the largest load of 7.654 nN; S, however, noticeably changes with temperature; see SM. Figures 2(c) and 2(e) depict the frictional stress, F_f/S—the force divided by the contact area. Its practical constancy is consistent with the assumption that friction force is proportional to the contact area, which is large enough (see SM). Moreover, the behavior of the friction coefficient, $\gamma = F_f/(SV_x)$ in Fig. 2(b) (inset) additionally supports this assumption; see also SM. Our simulations also confirm the lack of static friction. We do not compare the MD and experimental dependence of the friction force on the velocity, since the range of experimental and simulated velocities significantly differ (note that A°/ps = 100 m/s). Simulations demonstrate a linear dependence of friction force on the velocity, above some threshold velocity; see Figs. 2(b) and 2(d). The increase of the friction coefficient γ with increasing temperature T [see inset in Fig. 2(b)] indicates thermal mechanism of friction; see below and SM.

Theory.—Both experimental and simulation results evidence the thermal origin of the friction force—while surface corrugation, caused by the atomic potential, is very small for incommensurate contact, thermal fluctuations may cause much larger corrugation, hindering the relative motion of bodies at a contact. Here, we propose a mechanism that explains friction independence on the normal load. It also explains the observed velocity and temperature dependence of friction. In contrast to previous studies, which analyzed the role of thermal fluctuations in

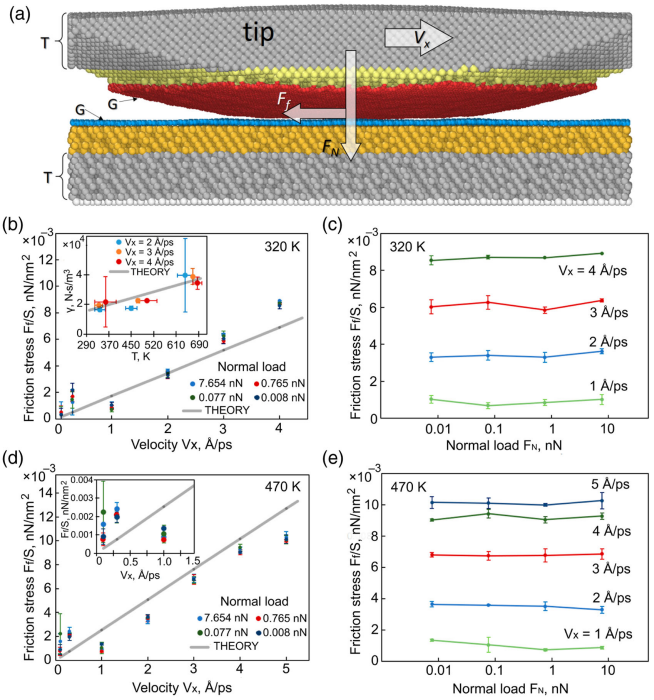

FIG. 2. The setup and results of MD simulations. (a) Graphene nanosheet (shown blue) is firmly adhered on the surface (111) of Cu substrate (orange and gray) and (shown red) on the copper tip (light yellow, gray, and white). The groups of atoms coupled to the thermostats of temperature T are given in gray. The positions of Cu atoms on the bottom substrate layer (white) are fixed. (b) The dependence of the frictional stress, F_f/S, where S is the area of the contact, on the tip's velocity V_x for the different normal load F_N at temperature $T \simeq 320$ K. The theoretical dependence, $F_f/S = \gamma V_x$, with γ given by Eq. (10) is shown by thick gray line. The single fitting parameter $(b\eta/Y) \simeq (8.5 \pm 1.5) \times 10^{-16}$ s is used, which yields the ratio $(\gamma/T) \simeq 54.0$ Ns/(K m^3). The inset shows the dependence of the friction coefficient, $\gamma = F_f/(SV_x)$, on temperature for the normal load of $F_N = 0.765$ nN. (c) Frictional stress F_f/S as the function of the normal load F_N for different tip velocities at 320 K. (d),(e) The same as for the main panels (b) and (c), respectively, but for $T \simeq 470$ K.

the context of Prandtl-Tomlinson model [5,55–57], we demonstrate that the major role for molecular smooth, incommensurate surfaces play surface fluctuations of a special type, when surfaces remain in a tight contact; we call them "synchronic fluctuations"; see Fig. 3. The energy of such fluctuations is significantly smaller than that of other surface fluctuations. Hence, the synchronic fluctuations, generated by thermal noise, can develop relatively large amplitudes, that is, they dominate. The respective surface corrugation effectively hinders the surface sliding, giving rise to the friction force.

To simplify the explanation of the basic mechanism, we consider here an idealized model of a contact in vacuum of two identical flat bodies with a uniform deformation. More rigorous analysis of the general case is presented in SM; it leads to the same conclusion. Let molecular smooth

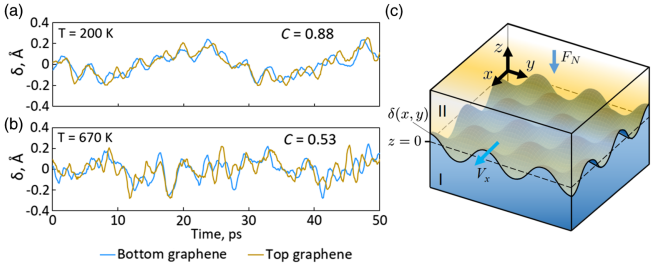

FIG. 3. The synchronicity of surface thermal fluctuations, responsible for friction, demonstrated by MD simulations. The time dependence of the vertical deviation $\delta(t)$ from the equilibrium plane $z = 0$ for the central segment of the bottom (blue) and upper (yellow) surfaces is shown for 200 K (a) and 670 K (b). The synchronicity is quantified by the correlation coefficient C ($C = 1$ for complete synchronicity); it decreases with increasing temperature; see SM for detail. (c) The schematic sketch of the synchronic thermal fluctuations.

surfaces of two such bodies, with the same elastic and other properties, be in a contact at the plane $z = 0$. Let the bodies be pressed together by the normal load F_N, directed along z axis; see Fig. 3. If the area of the contact is S, than the normal stress $\sigma_{zz} = F_N/S$ emerges at $z = 0$. It yields the equilibrium deformation of $u_{zz}^{(1)}$ of the first body and $u_{zz}^{(2)}$ of the second body, such that $u_{zz}^{(1)} = u_{zz}^{(2)} = u_{zz}^{\rm eq} = Y^{-1}\sigma_{zz}$, where Y is the Young modulus of the material [58]. (Note that the continuum mechanics concepts remain applicable at the nanoscale; see, e.g., [59]). Then the deformation energy of the two bodies at equilibrium reads [58]

$$E_{\rm eq} \simeq 2\frac{1}{2}\int u_{zz}^{\rm eq}\sigma_{zz}d\mathbf{r} = Y(u_{zz}^{eq})^2 SL, \tag{1}$$

where the integration is performed over the whole volume of the bodies, equal to SL, with L being their dimension in the direction along z axis. Consider now a small deviation, $\pm\delta(x, y)$, of both surfaces from the equilibrium position at $z = 0$, such that the surfaces remain in a tight contact. These deviations correspond to the synchronic fluctuations; see Fig. 3. The respective deformations are

$$u_{zz}^{(1)} = u_{zz}^{\rm eq} + \tilde{\delta}(x, y), \qquad u_{zz}^{(2)} = u_{zz}^{\rm eq} - \tilde{\delta}(x, y), \tag{2}$$

where $\tilde{\delta}(x, y) = \delta(x, y)/L$ is the deformation caused by the surface fluctuation $\delta(x, y)$. The energy of the synchronic fluctuation then reads

$$\begin{aligned}\delta E &= \frac{Y}{2}\int d\mathbf{r}\left[\left(u_{zz}^{\rm eq} + \tilde{\delta}(x, y)\right)^2 + \left(u_{zz}^{\rm eq} - \tilde{\delta}(x, y)\right)^2\right] - E_{\rm eq} \\ &= (Y/L)\int_S dxdy\,\delta^2(x, y),\end{aligned} \tag{3}$$

that is, $\delta E = \mathcal{O}(\delta^2)$, which means that the energy of such synchronic fluctuations are second order with respect to the amplitude δ. The lack of linear-order terms in the fluctuations energy, δE, makes them much more energetically favorable than nonsynchronic fluctuations, whose energy contains linear-order terms in δ. Hence, the synchronic fluctuations play a major role in thermal corrugation of the surface, providing the main friction mechanism for incommensurate surfaces. The dominance of synchronic fluctuations is directly confirmed by numerical simulations; see Fig. 3.

Even more important is that the fluctuation energy δE does not depend on the equilibrium deformation $u_{zz}^{\rm eq}$, that is, it is independent on the normal load, F_N. Hence, we come to the principle conclusion: the friction force (for this type of superlubricity) is mainly determined by the surface corrugation, due to synchronic fluctuations, and does not depend on the normal load.

Now we estimate the dependence of the friction force F_f on the relative velocity V of the surfaces. We will not discuss here the dependence F_f for small velocities, but will address the velocities larger than a threshold velocity V_*, which may be associated with the propagation velocity of the synchronic fluctuations along the surface. Based on the estimates detailed in SM, we obtain, $V_* \sim 50$–100 m/s.

Consider the dissipation of energy due to relative motion of two surfaces with the velocity $V > V_*$. We assume that for $V > V_*$, the surfaces, corrugated by the synchronic fluctuations, remain in a tight contact, so that

$$u_{zz}^{(1/2)}(x, y, t) = u_{zz}^{\rm eq} \pm \tilde{\delta}(x - Vt, y). \tag{4}$$

This means that the sliding motion "drives the wrinkles" of the synchronic fluctuations in the direction of the relative motion; see Fig. 3(c). Then the deformation $u_{zz}^{(1/2)}(x, y, t)$ varies in time as

$$\frac{d}{dt}u_{zz}^{(1)} = -\frac{V}{L}\frac{\partial}{\partial x}\delta(x, y), \qquad \frac{d}{dt}u_{zz}^{(2)} = \frac{V}{L}\frac{\partial}{\partial x}\delta(x, y), \tag{5}$$

yielding the dissipation of energy per unit time $W_{\rm diss}$. It is quantified by the dissipative function R [58]. In our case all deformation components except u_{zz} may be neglected, which yields (see SM for more detail)

$$\begin{aligned}R &= \eta\left(\frac{du_{zz}^{(1)}}{dt}\right)^2 + \eta\left(\frac{du_{zz}^{(2)}}{dt}\right)^2, \\ W_{\rm diss} &= \int R\,d\mathbf{r} = \left(\frac{2\eta}{L}\right)V^2\int_S\left(\frac{\partial\delta(x, y)}{\partial x}\right)^2 dxdy.\end{aligned} \tag{6}$$

Here, $\eta = (\frac{4}{9}\eta_1 + \frac{1}{2}\eta_2)$, with η_1 and η_2 being the viscosity coefficients of solid material, quantifying viscous losses, respectively, for shear and bulk deformation rates [58].

Since the thermal fluctuations, $\delta(x, y)$, are random, the averaging of $W_{\rm diss}$ is needed. It may be done using the probability of such fluctuations, $P(\delta) = Z^{-1}e^{-E(\delta)/k_BT}$,

where $E(\delta(x,y))$ is the energy of the fluctuation $\delta(x,y)$, T is temperature, k_B the Boltzmann constant, and Z^{-1} the normalization factor. The averaging is to be performed over all possible $\delta(x,y)$:

$$\langle W_{\rm diss}\rangle = \int \mathcal{D}[\delta(x,y)] W_{\rm diss}[\delta(x,y)] P[\delta(x,y)]. \quad (7)$$

$\mathcal{D}[\delta(x,y)]$ in (7) denotes functional integration over two-dimensional functions, associated with the surface fluctuations at the contact area S. Note that Eq. (7) shows that $\langle W_{\rm diss}\rangle$ does not depend on the normal load. Indeed, $E(\delta)$, and hence $P(\delta)$ in Eq. (7), do not depend on $F_{\rm N}$. Referring for computation details to SM (where it is done for the general model), we present the final result:

$$\langle W_{\rm diss}\rangle = F_{\rm f} V = \pi b (k_B T/Y) \rho_s^2 \eta V^2 S, \quad (8)$$

where ρ_s is the number of surface atoms per unit area and we take into account that the dissipation power is equal to the product of the velocity V and friction force $F_{\rm f}$. The numerical coefficient b depends on the Poisson ratio ν and combination of viscous constants $r = (\frac{4}{9} + \frac{1}{2}\eta_2/\eta_1)^{-1}$ as

$$b = \frac{(1+\nu)(1-2\nu)}{\pi^2}\left[\frac{b_1 + r b_2}{b_2 + (1-\nu) b_1}\right], \quad (9)$$

where we abbreviate, $b_1 \equiv 5\text{–}8\nu + 8\nu^2$ and $b_2 \equiv 13\text{–}20\nu + 8\nu^2$; see SM. This yields the friction force and coefficient

$$F_{\rm f} = \gamma S V, \qquad \gamma = \pi b (k_B T/Y) \rho_s^2 \eta. \quad (10)$$

Hence, we demonstrate that the friction force does not depend on the normal load, in a qualitative agreement with the experiment and simulations, Figures 1 and 2 explain the atomistic mechanism of this phenomenon. We also show that it linearly depends on the sliding velocity V and contact area S, while the friction coefficients γ linearly increase with temperature, in agreement with the numerical experiments; see Figs. 2(b)–2(e). Note that the friction coefficient γ is expressed in terms of the square average of thermal synchronic fluctuations, $\gamma \sim \langle W_{\rm diss}\rangle \sim \eta \langle (\partial\delta/\partial x)^2\rangle$, that is, it obeys the fluctuation-dissipation relation [60,61]; a similar linear dependence on T of the dynamic friction force was reported for double-wall nanotubes [27].

Conclusion.—We explore dynamic structural superlubricity experimentally and numerically, using incommensurate contact of two solid surfaces with firmly adhered graphene layers. The contact area was relatively large, corresponding to "solitonlike smooth sliding" regime, by the classification of Ref. [19], where friction force is proportional to the contact area. We observe superlubric behavior for a wide range of the normal load and relative velocities of surfaces, spanning several orders of magnitude. The impact of temperature has been also investigated. For this kind of superlubricity we propose a few friction laws and support them by theoretical analysis. In contrast to conventional Amontons-Coulomb laws of dry friction [1,2], we demonstrate independence of friction force on the normal load and its increase with increasing intersurface velocity and temperature. Furthermore, we show that above some threshold velocity the dependence of friction force on the velocity is linear; the temperature dependence is also linear. We propose an atomistic mechanism of friction independence on the normal load in terms of synchronic out-of-plane surface fluctuations of thermal origin, when two surfaces remain in a tight contact. Because of relatively small energy, such fluctuations dominate, yielding corrugation of the contacting surfaces, which hinders the relative motion. We confirm this mechanism in our MD experiments. We show that the intensity of such synchronic fluctuations, which determine friction, does not depend on the normal load. As the result, friction force does not depend on the normal load for both small velocities (as in the experiment) and large ones (as in MD simulations). For large velocities (exceeding the propagation velocity of synchronic fluctuations) we develop a theory of the friction force. It is in fair agreement with the simulation data. We show that the friction coefficient obeys the fluctuation-dissipation relation, which is similar to bulk viscous friction but is very unusual for conventional dry friction.

We thank Michael Urbakh for valuable comments and drawing our attention to Refs. [16,22]. A. G. N. acknowledges the Ministry of Science and Higher Education of the Russian Federation (Project No. FZSR-2020-0007, FZSR-2024-0004).

[1] V. L. Popov, *Contact Mechanics and Friction. Physical Principles and Applications*, 2-nd ed. (Springer, Berlin, 2017).
[2] C. D. A. Berman and J. Israelachvili, Tribol. Lett. **4**, 95 (1998).
[3] K. Holmberg and A. Erdemir, Friction **5**, 263 (2017).
[4] K. Sayfidinov, S. D. Cezan, B. Baytekin, and H. T. Baytekin, Sci. Adv. **4**, 3808 (2018).
[5] A. Vanossi, N. Manini, M. Urbakh, S. Zapperi, and E. Tosatti, Rev. Mod. Phys. **85**, 529 (2013).
[6] K. M. Sankar, D. Kakkar, S. Dubey, S. V. Garimella, M. Goyat, S. Joshi, and J. K. Pandey, Proc. Instn. Mech. Engrs. J **234**, 448 (2020).
[7] M. Hirano and K. Shinjo, Phys. Rev. B **41**, 11837 (1990).
[8] K. Shinjo and M. Hirano, Surf. Sci. **283**, 473 (1993).
[9] M. Dienwiebel, G. S. Verhoeven, N. Pradeep, J. W. M. Frenken, J. A. Heimberg, and H. W. Zandbergen, Phys. Rev. Lett. **92**, 126101 (2004).

[10] M. Dienwiebel, N. Pradeep, G. S. Verhoeven, H. W. Zandbergen, and J. W. M. Frenken, Surf. Sci. **576**, 197 (2005).

[11] E. Koren, E. Lortscher, C. Rawlings, A. W. Knoll, and U. Duerig, Science **348**, 679 (2015).

[12] Z. Liu, J. Yang, F. Grey, J. Z. Liu, Y. Liu, Y. Wang, Y. Yang, Y. Cheng, and Q. Zheng, Phys. Rev. Lett. **108**, 205503 (2012).

[13] C. C. Vu, S. Zhang, M. Urbakh, Q. Li, Q. C. He, and Q. Zheng, Phys. Rev. B **94**, 081405(R) (2016).

[14] Y. Song, D. Mandelli, O. Hod, M. Urbakh, M. Ma, and Q. Zheng, Nat. Mater. **17**, 894 (2018).

[15] D. Mandelli, I. Leven, O. Hod, and M. Urbakh, Sci. Rep. **7**, 10851 (2017).

[16] D. Mandelli, W. Ouyang, O. Hod, and M. Urbakh, Phys. Rev. Lett. **122**, 076102 (2019).

[17] E. Koren and U. Duerig, Phys. Rev. B **94**, 045401 (2016).

[18] O. Hod, E. Meyer, Q. Zheng, and M. Urbakh, Nature (London) **563**, 485 (2018).

[19] D. Mandelli, I. Leven, O. Hod, and M. Urbakh, Sci. Rep. **7**, 10851 (2017).

[20] A. S. Minkin, I. V. Lebedeva, A. M. Popov, and A. A. Knizhnik, Phys. Rev. B **104**, 075444 (2021).

[21] Z. Liu, J. Yang, F. Grey, J. Z. Liu, Y. Liu, Y. Wang, Y. Yang, Y. Cheng, and Q. Zheng, Phys. Rev. Lett. **108**, 205503 (2012).

[22] A. E. Filippov, M. Dienwiebel, J. W. M. Frenken, J. Klafter, and M. Urbakh, Phys. Rev. Lett. **100**, 046102 (2008).

[23] W. K. Kim and M. L. Falk, Phys. Rev. B **80**, 235428 (2009).

[24] M. Ma, A. Benassi, A. Vanossi, and M. Urbakh, Phys. Rev. Lett. **114**, 055501 (2015).

[25] W. Ouyang, M. Ma, Q. Zheng, and M. Urbakh, Nano Lett. **16**, 1878 (2016).

[26] J. Servantie and P. Gaspard, Phys. Rev. Lett. **91**, 185503 (2003).

[27] I. Lebedeva, A. Knizhnik, A. Popov, Y. Lozovik, and B. Potapkin, Nanotechnology **20**, 105202 (2009).

[28] K. B. Jinesh, S. Y. Krylov, H. Valk, M. Dienwiebel, and J. W. M. Frenken, Phys. Rev. B **78**, 155440 (2008).

[29] K. B. Jinesh, S. Y. Krylov, H. Valk, M. Dienwiebel, and J. W. M. Frenken, Phys. Rev. B **78**, 155440 (2008).

[30] Q. Li, Y. Dong, D. Perez, A. Martini, and R. W. Carpick, Phys. Rev. Lett. **106**, 126101 (2011).

[31] J. Norell, A. Fasolino, and A. S. de Wijn, Phys. Rev. E **94**, 023001 (2016).

[32] H. Lee, N. Lee, Y. Seo, J. Eom, and S. Lee, Nanotechnology **20**, 325701 (2009).

[33] D. Berman, A. Erdemir, A. V. Zinovev, and A. V. Sumant, Diamond Relat. Mater. **54**, 91 (2015).

[34] L.-Y. Lin, D.-E. Kim, W.-K. Kim, and S.-C. Jun, Surf. Coat. Technol. **205**, 4864 (2011).

[35] See Supplemental Material, which includes Refs. [36–46], at http://link.aps.org/supplemental/10.1103/PhysRevLett.131.266201 where we present the detailed description of the experimental setup and methods, details of the MD simulations and of the theoretical derivation of the friction force.

[36] A. Feiler, P. Jenkins, and M. W. Rutland, J. Adhes. Sci. Technol. **19**, 165 (2005).

[37] X. Zhao and S. S. Perry, ACS Appl. Mater. Interfaces **2**, 1444 (2010).

[38] T. Arif, G. Colas, and T. Filleter, ACS Appl. Mater. Interfaces **10**, 22537 (2005).

[39] V. E. P. Claerbout, P. Nicolini, and T. Polcar, Front. Chem. **9**, 684441 (2021).

[40] S. Plimpton, J. Comput. Phys. **117**, 1 (1995).

[41] R. P. Feynman, *Statistical Mechanics: A Set Of Lectures* (Avalon Publishing, New York, 1998).

[42] N. Brilliantov, Y. A. Budkov, and C. Seidel, Faraday Discuss. **199**, 487 (2017).

[43] S. P. Timoshenko, *Theory of Elasticity* (McGraw-Hill, New York, 1970).

[44] Lammps documentation, https://docs.lammps.org/fix_temp_rescale.html.

[45] A. Tsukanov, Models for project nanofriction at github.

[46] N. W. Ashcroft and N. D. Mermin, *Solid State Physics* (Holt, Rinehart and Winston, 1976).

[47] A. K. Grebenko, D. V. Krasnikov, A. V. Bubis, V. S. Stolyarov, D. V. Vyalikh, A. A. Makarova, A. Fedorov, A. Aitkulova, A. A. Alekseeva, E. Gilshtein, Z. Bedran, A. N. Shmakov, L. Alyabyeva, R. N. Mozhchil, A. M. Ionov, B. P. Gorshunov, K. Laasonen, V. Podzorov, and A. G. Nasibulin, Adv. Sci. **9**, 2200217 (2022).

[48] D. W. Brenner, O. A. Shenderova, J. A. Harrison, S. J. Stuart, B. Ni, and S. B. Sinnott, J. Phys. Condens. Matter **14**, 783 (2002).

[49] W. Ouyang, D. Mandelli, M. Urbakh, and O. Hod, Nano Lett. **18**, 6009 (2018).

[50] A. N. Kolmogorov and V. H. Crespi, Phys. Rev. B **71**, 235415 (2005).

[51] M. S. Daw and M. I. Baskes, Phys. Rev. Lett. **50**, 1285 (1983).

[52] M. S. Daw and M. I. Baskes, Phys. Rev. B **29**, 6443 (1984).

[53] Y. Mishin, M. Mehl, D. Papaconstantopoulos, A. Voter, and J. Kress, Phys. Rev. B **63**, 224106 (2001).

[54] P. Süle and M. Szendrő, Model. Simul. Mater. Sci. Eng. **23**, 025001 (2014).

[55] E. Gnecco, R. Bennewitz, T. Gyalog, Ch. Loppacher, M. Bammerlin, E. Meyer, and H.-J. Güntherodt, Phys. Rev. Lett. **84**, 1172 (2000).

[56] M. Weiss, L. Majchrzycki, E. Borkowska, and M. Cichomski, Tribol. Int. **162**, 107133 (2021).

[57] J. Chen, I. Ratera, J. Y. Park, and M. Salmeron, Phys. Rev. Lett. **96**, 236102 (2006).

[58] L. D. Landau and E. M. Lifshitz, *Theory of Elasticity* (Oxford University Press, Oxford, 1965).

[59] K. Saitoh, A. Bodrova, H. Hayakawa, and N. V. Brilliantov, Phys. Rev. Lett. **105**, 238001 (2010).

[60] P. Resibois and M. de Leener, *Classical Kinetic Theory of Fluids* (Wiley & Sons, New York, 1977).

[61] W. Ebeling and I. M. Sokolov, *Statistical Thermodynamics and Stochastic Theory of Nonequilibrium Systems* (World Scientific, Singapore, 2005).